

Design and Simulation of Broadband Horn Nanoantennas for Nanophotonic Applications

Larissa da Silva Brito , Raquel Aline Araújo Rodrigues Felix 

Department of Electrical Engineering, Federal University of Campina Grande, Campina Grande, Brazil
larissa.brito@ee.ufcg.edu.br, raquel@dee.ufcg.edu.br

Abstract— Optical plasmonic nanoantennas have proven useful in nanoplasmonic applications, paving the way for more efficient wireless optical communications. In this work, we propose a parametric study of a plasmonic horn nanoantenna in flat H sectorial format and beveled horn, both designed to radiate in the three wavelengths of optical communications: [850 nm (352.9 THz), 1310 nm (229 THz) and 1550 nm (193.5 THz)]. The modeling of the chosen nanoantennas was performed in COMSOL Multiphysics version 6.0. The simulation results prove that the geometries presented satisfactory results of reflection coefficient and gain. In addition, to complement the parametric study, the conductive metal (in gold, silver and aluminum) was varied for each nanoantenna. Through the study, it was noticed that the nanostructures simulated in silver and aluminum are potential for applications in optical nanolinks and energy harvesting.

Index Terms— H-plane Sectorial Horn Nanoantenna; Parametric Study; Computational Simulation.

I. INTRODUCTION

With the development of research and nanostructured materials, nanophotonics has become an enormous technological potential. The successful applications of nanostructured materials is due to the fact that their optical properties are related to their interaction with electromagnetic radiation (photons). And so, the study of the phenomena of absorption, emission, reflection and refraction allows us to know how each material behaves [1]. Therefore, nanophotonics is a field of science that aims to study the optical properties of materials at the nanoscale [2].

In the last two decades, nanoplasmonics has become a very significant research target in technological applications [3]. As an emerging technology, nanoplasmonics has profoundly impacted the performance of several promising research projects, bringing new and exciting challenges in modern science [4]. Among the several recent applications of nanoplasmonics, the following stand out: plasmonic biosensors [5]-[10]; plasmonic photocatalysis [11]-[13]; plasmonic devices such as photodetectors [14]-[16]; and lasers [17] and [18].

Although great achievements have been made through the control of light in various scopes, manipulation of light direction at the sub-wavelength scale with conventional optical devices is still a challenge [19]. The main difficulty encountered when controlling light at the nanoscale is the diffraction limit of light, where the smallest resolvable characteristic is at the wavelength scale [20].

In this sense, the design of plasmonic nanoantennas stands out for being able, through the optical properties of light manipulation, to overcome the challenges between the microscopic and macroscopic scales due to the resonant properties [21] and [22].

The first plasmonic nanostructures were used as optical nanostructures, and since then they have been widely used to redirect light scattering and emission, as they have excellent directional light scattering properties [20]. Among the numerous applications of nanoantennas in the literature, their integration in optical chip applications [23] and [24] stands out; wireless optical nanolink [25] and [26]; biosensors [27] and [28]; nanocircuits [29], [30]; anti-reflective coating [31], solar energy harvesting [32], at the same time spectral and spatial separation of light [33] and [34]; and hydrogen detection [35].

Since 2021, several scientific articles have been invading their applications of plasmonic nanoantennas. For example, in the work of [36], the authors argue that plasmonic nanoantennas can be designed to generate directional hypersonic surface acoustic waves. This can be valuable for integrated optical circuits, where the addition of an acoustic element can decrease the wavelength at the same operating frequency as the incident electromagnetic wave. The authors of [37], on the other hand, developed a project of an optical energy collector to power wireless IoT sensors.

But among the many innovations, the work of [38] draws attention due to the proposal of an optical nano-antenna in the shape of a maple leaf inspired by nature, which is presented and fed with a hybrid plasmonic waveguide. The design proposed by the researchers provides a high gain of 11.8 dB at THz frequencies and a bandwidth of 400 GHz. In addition, the proposal can be used for optical energy capture applications with satisfactory performance. The nanoantenna powered by a circular hybrid plasmonic waveguide of [39] proved to be useful for on-chip wireless optical communications and its performance was investigated numerically and theoretically. Another interesting recent proposal is the rectenna designed in [40], the rectenna consists of a conical gold antenna coupled to an insulating metallic substrate that captures electromagnetic radiation. The rectenna proposed by the authors has also been shown to operate at 384 THz (780 nm), paving the way for efficient rectennas.

It is noted that recent studies of plasmonic nanoantennas for nanophotonic applications are merely individual studies, in other words, they do not consist of a defined parametric study, but rather focus on specific models. Therefore, the research differential consists in filling the gaps of a more complete and comparative study, analyzing the influence of the geometry and materials chosen for the design of plasmonic horn nanoantennas.

In this way, the work was organized through a parametric study involving two geometries (H-plane sectorial horn and beveled horn), in addition, the variation of three conductive metals (gold [Au], silver [Ag] and aluminum [Al]) was analyzed, in the three distinct frequencies of the optical spectrum (193.5 THz, 229 THz and 352.9 THz). Although most researchers use gold or silver to manufacture nanoantennas, the results obtained in this article show that aluminum can have even better results than other types of materials, mainly due to its reflection coefficient as observed in [41]. Thus, the

simulation environment chosen was a commercial computational platform and the results were obtained and compared in terms of reflection coefficient, gain and directivity. Therefore, in Section II the design of the plasmonic horn nanoantenna is presented. Section III describes the scenario and parameters used in the simulations. In Section IV, the results are shown and discussed and, finally, in Section V, the conclusions of this work are presented.

II. NANOANTENNAS DESIGN

Numerical results were obtained using the Finite Element Method (FEM) within the commercial software COMSOL Multiphysics 6.0. The broadband optical nanoantennas proposed for this work are based on the hybrid plasmonic structure [42]. Fig. 1 shows the basic geometry of the plasmonic waveguide and the basic shape of the H plane sector horn and bevel horn nanoantenna used during the simulations.

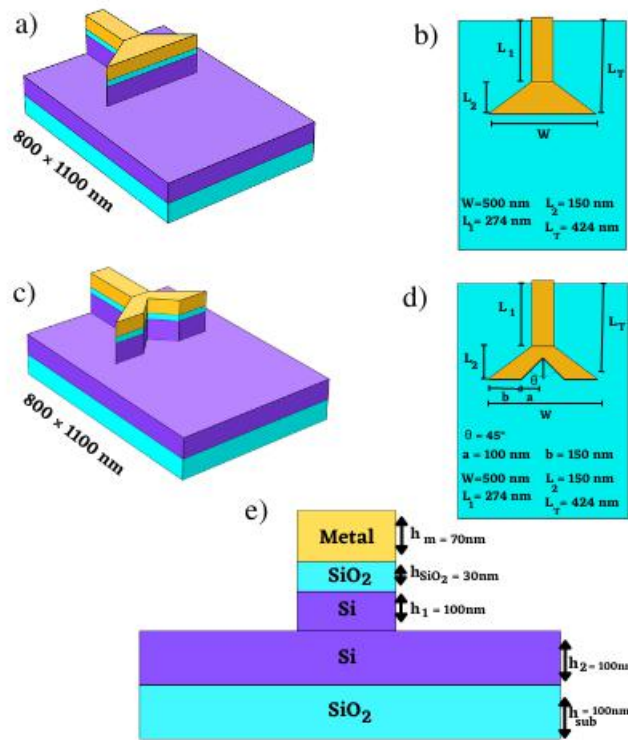


Fig. 1. Dimensions of the nanoantennas used in this work, H-plane sectoral horn and beveled horn, considering the views: (a) and (c) 3D; (b) and (d) superior of the nanoantennas and (e) transversal.

The nanoantennas were chosen based on the literature [43], with the purpose of contemplating the format, the implementation of a material with a low refractive index (such as SiO_2), a metallic layer that was varied between gold, silver and aluminum and still a layer material with a higher refractive index (Si). The nanoantenna is powered by a hybrid plasmonic waveguide layered with different materials. At the top of the structure is located the metallic layer of the antenna whose thickness was initially delimited from $h_m = 70$ nm, after the conductive layer was introduced a layer of material with a lower refractive index of silicon dioxide with a thickness of $h_{\text{SiO}_2} = 30$ nm, this layer is sandwiched

between metal and silicon layer, whose thickness is $h_1 = 100\text{nm}$ and then by $h_2 = 100\text{nm}$. The substrate height (h_{sub}) is initially set to 100 nm. For the beveled horn, a 45° opening was made in the nanoantenna, keeping the values fixed at $a=100\text{ nm}$ and $b=150\text{ nm}$. The parameters of $L_T=424\text{ nm}$, $L_1 = 274\text{ nm}$, $L_2 = 15\text{nm}$ and $w = 500\text{ nm}$ were maintained for any variation in thickness, metal and nanoantenna geometry throughout the parametric study. In order to cover all optical communication windows, we have fixed our frequency range between 150–400 THz.

III. MODELING AND SIMULATION METHOD

During the research, the modeling of the proposed nanoantennas was carried out in the COMSOL Multiphysics 6.0 simulation environment through the module specially designed for the propagation of electromagnetic waves, the RF (radio frequency). The software uses the Finite Element Method (FEM) to model and calculate the study variables.

During the simulations, after the step of structuring the geometry of the nanoantennas, the definition of the materials that compose the structure was made using the internal library of materials available on the Comsol's platform.

After defining the physical constants of the materials, the boundary conditions were implemented using Frequency Domain physics (i.e., in time-harmonic regime), since with it is possible to calculate resonance frequencies, S parameters, near/far fields, gain and directivity. In addition, a numerical gate feature was added at the ends of the nanoantenna layers to calculate the dispersion parameters (S parameters). In this case, the number gate is intended to analyze the electric field at the gate boundary (i.e., the longitudinal normal component parallel to the propagation direction) as a TEM mode. In Fig. 2 it is possible to see an illustration of the models of the horn nanoantenna (a) H-plane sectorial and (b) beveled.

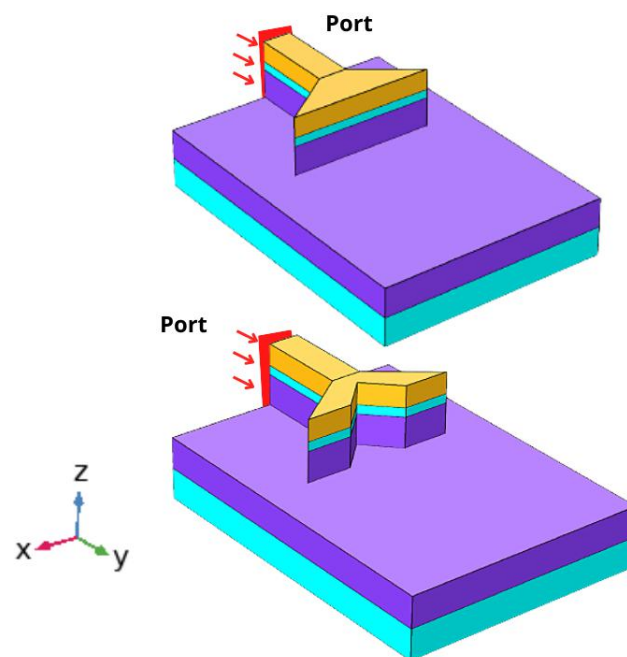


Fig. 2. Feeding the horn nanoantenna: (a) H-plane sectorial and (b) beveled.

Note the red arrows indicating the power flow from the port, which presumably must be in the -y direction. The nanoantenna feed was done in addition to the conductive metal layer, this is because the gates need to be large enough to fully capture the mode of interest, including marginal fields. An irregular configuration of the power flow of the ports may cause no electromagnetic wave to be transmitted through the port.

IV. RESULTS AND DISCUSSION

In this section, the results of the simulations of the parametric study are presented, varying the geometry of the proposed nanoantenna, the conductive metal and the thickness of the layers that compose the plasmonic waveguide. Fig. 3 illustrates the discretized meshes in the solution domain for the (a) H-plane sectorial horn and (b) beveled horn antennas.

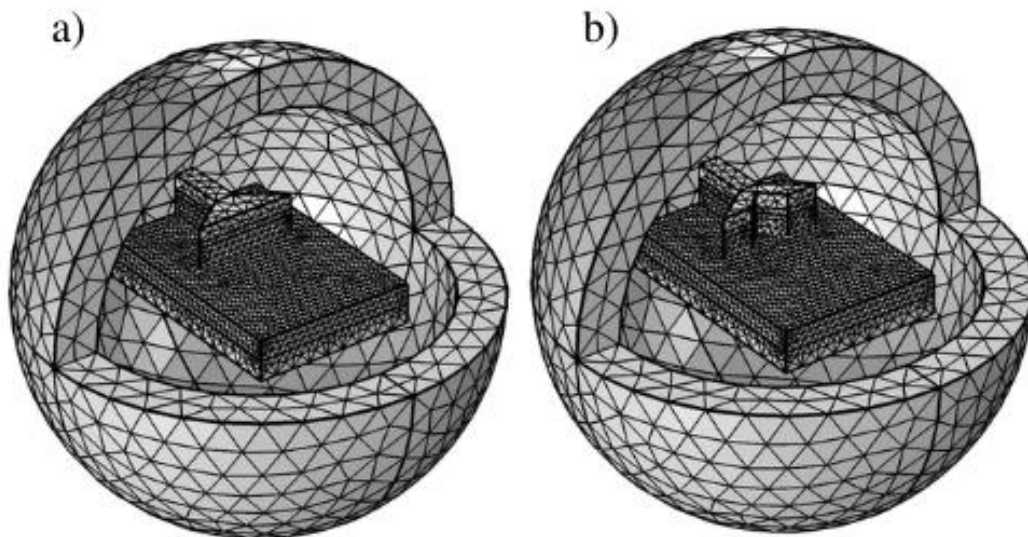


Fig. 3. Mesh discretization results for the models: (a) H-plane sectorial horn and (b) beveled horn.

The mesh option performed was chosen as refined as possible on the surfaces of greatest interest - power supply and dielectric - reducing the computational cost for the model solution. Fig. 4 shows the electric field distribution along the plasmonic waveguide obtained using the Port resource in the antenna feed. The electric field is concentrated in the SiO₂ layer, confirming the excitation of the hybrid plasmonic TM mode [44]. It can be seen through the color legend on the right that the electric field norm reached maximum values (in blue and red highlights) in the feed layers of the guide close to the metal and dielectric. To support the fundamental TM mode and provide a perfect impedance match between the antenna and the waveguide, the width of the SiO₂ coating layer was chosen as 100 nm.

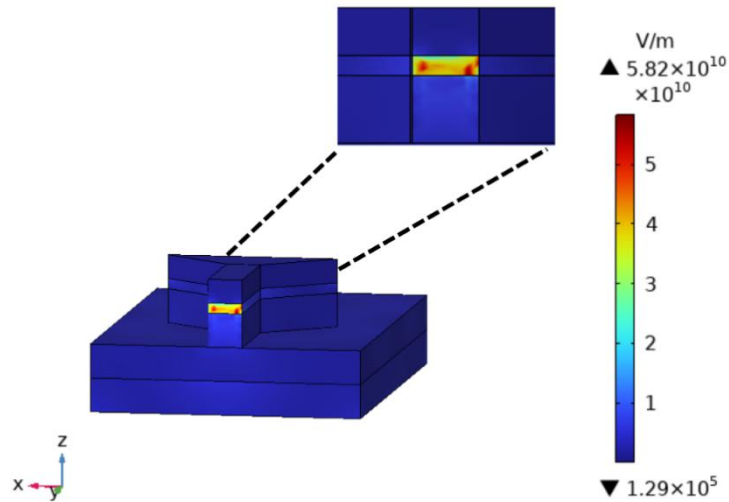


Fig. 4. Electric field distribution in the H-plane sectorial horn nanoantenna guide.

A. H-plane sectorial horn nanoantenna

The 3D radiation graphs at optical communications frequencies for the H-plane sectorial horn nanoantenna with conductive metal in gold, silver and aluminum are shown in Fig. 5, 6 and 7, respectively.

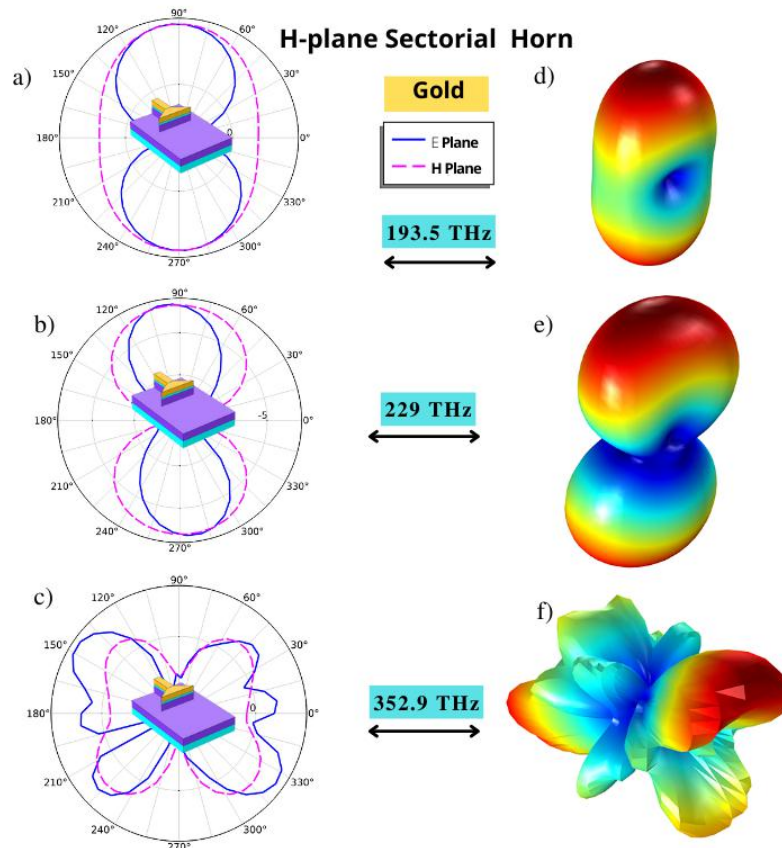


Fig. 5. H-plane sectorial horn radiation diagrams in gold: in 2D (a), (b) and (c); and in 3D (d), (e) and (f).

H-plane Sectorial Horn

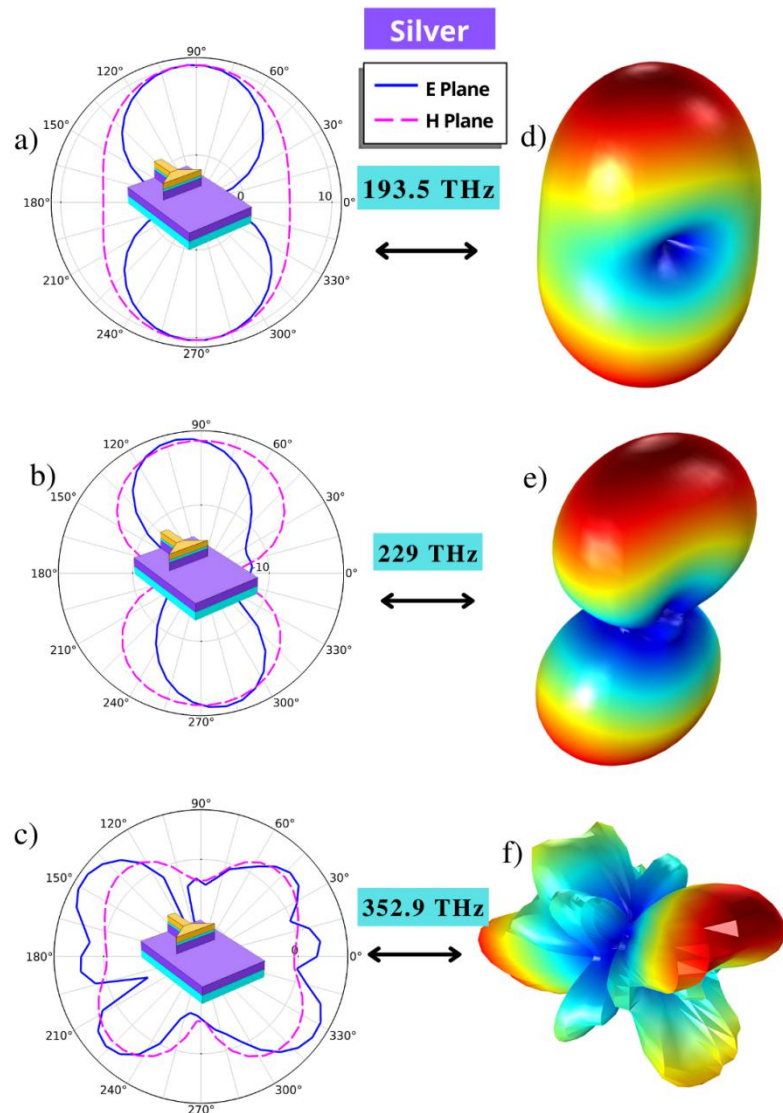


Fig. 6 H-plane sectorial horn radiation diagrams in gold: in 2D (a), (b) and (c); and in 3D (d), (e) and (f).

From Figs. 5, 6 and 7, it is noted that as the transmission frequency increases, the antenna beam width decreases and the antenna becomes less directive. Table I shows the results of the parameters: directivity, reflection coefficient and nanoantenna gain.

Fig. 8 shows the results of the reflection coefficient (S_{11}) as a function of frequency, for the simulated H-plane sector horn with radiating element in gold (Au), silver (Ag) and aluminum (Al). The pink dashed line delimits a better reflection coefficient for the nanoantenna, which constitutes values below -10 dB.

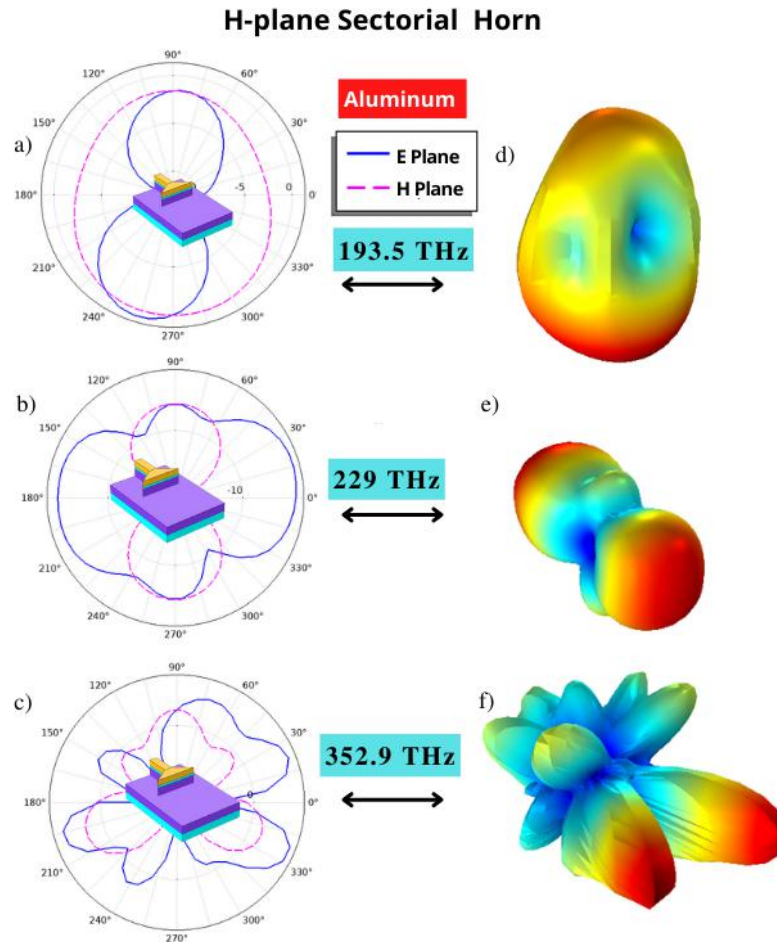


Fig. 7. H-plane sectorial horn radiation diagrams in aluminum: in 2D (a), (b) and (c); and in 3D (d), (e) and (f).

TABLE I. RESULTS OF S_{11} , DIRECTIVITY AND GAIN OF THE H-PLANE SECTORIAL HORN

Metal	Parameters (dB)	193.5 THz	229 THz	352 THz
Au	S_{11}	-11.44	-11.46	-11,22
	Gain	8.19	-1.54	12.01
Ag	S_{11}	-15.00	-15.10	-18.50
	Gain	10.90	-1.98	13.29
Al	S_{11}	-25.35	-26.07	-22.00
	Gain	0.70	-1.21	12.01

Table I shows that the H plane sector horn with a metallic conductive layer in silver and aluminum presented better reflection coefficient values at the three simulated frequencies in relation to its gold counterpart. While the aluminum and silver nanoantenna also obtained excellent gain results at the frequency of 352 THz, with 12 and 13.29 dB, respectively. In this way, the sectorial horns with higher frequency act with better gain values than the others.

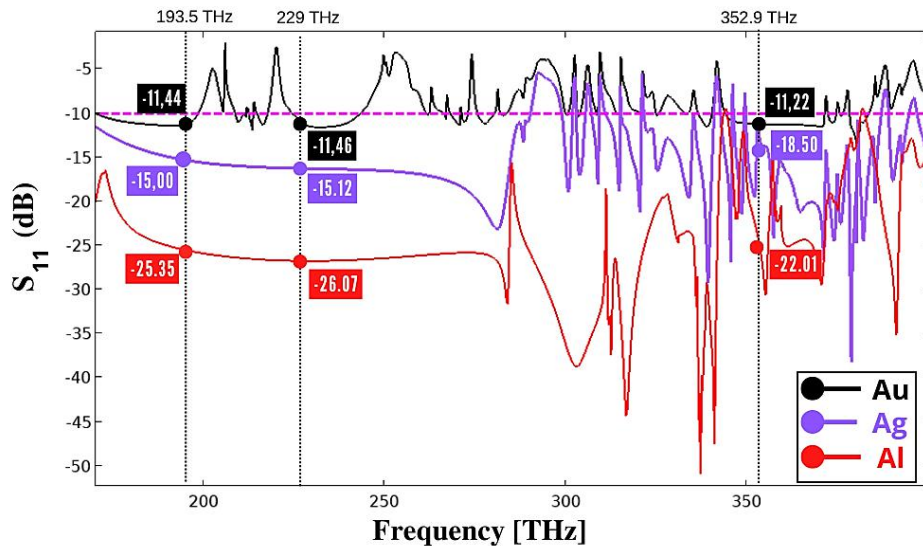


Fig. 8 Results of reflection coefficients (S_{11}) as a function of frequency for the H-plane sectorial horn in (Au), silver (Ag) and aluminum (Al).

A better match of the antenna and the power supplied to the H plane sectorial horn of aluminum is observed in relation to the gold and silver metals. Thus, for the H-plane sectorial horn in aluminum, it is noted that the impedance matching between the antenna and the guide is considered very good in relation to geometries with other conductive materials.

B. Beveled Horn Nanoantenna

Similarly, the 3D radiation plots, at optical communications frequencies, for the gold, silver and aluminum conductive metal beveled horn nanoantenna are shown in Fig. 10, 11 and 12, respectively. In Fig. 12, it is possible to visualize the results of reflection coefficient (S_{11}) as a function of frequency, for the beveled horn with radiating element in gold (Au), silver (Ag) and aluminum (Al). The coefficient values of each horn were highlighted on the graph for better understanding and association of results. In black, the reflection coefficient graph of the beveled horn with conductive metal in gold stands out, while in lilac and red, they refer respectively to the coefficients of the same geometry with conductive metal in silver and aluminum. There is a similarity between the silver and aluminum curves in relation to the gold curve, whose results remained closer to the value of -10 dB.

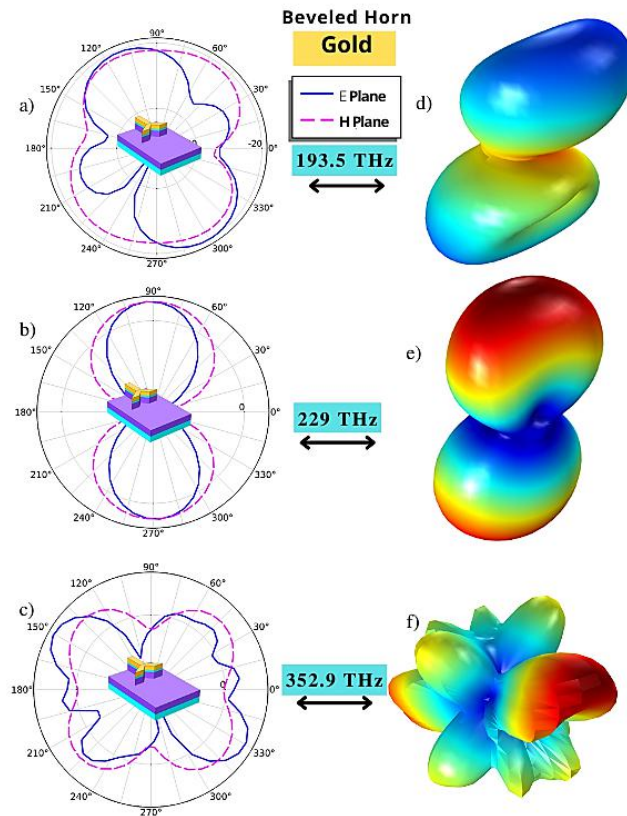


Fig. 9. Radiation diagrams of the beveled horn in gold: in 2D (a), (b) and (c); and in 3D (d), (e) and (f).

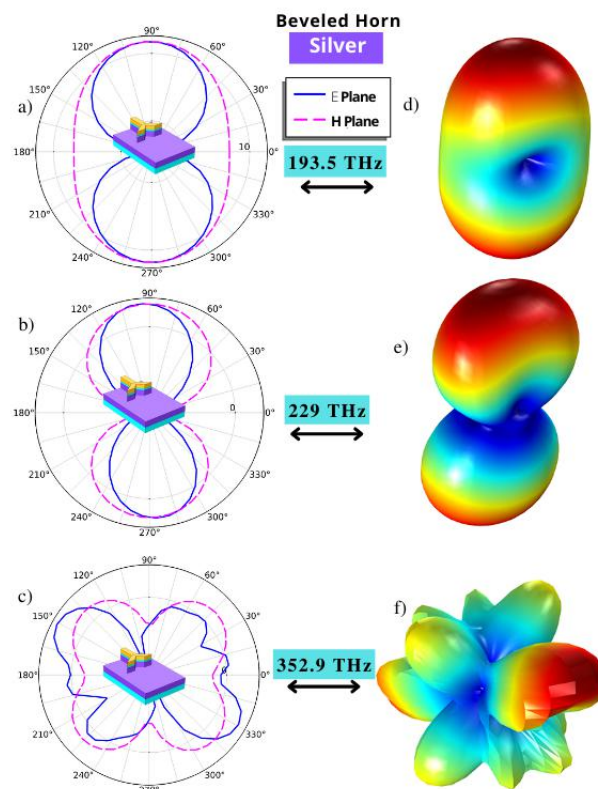


Fig. 10. Silver beveled horn radiation diagrams: in 2D (a), (b) and (c); and in 3D (d), (e) and (f).

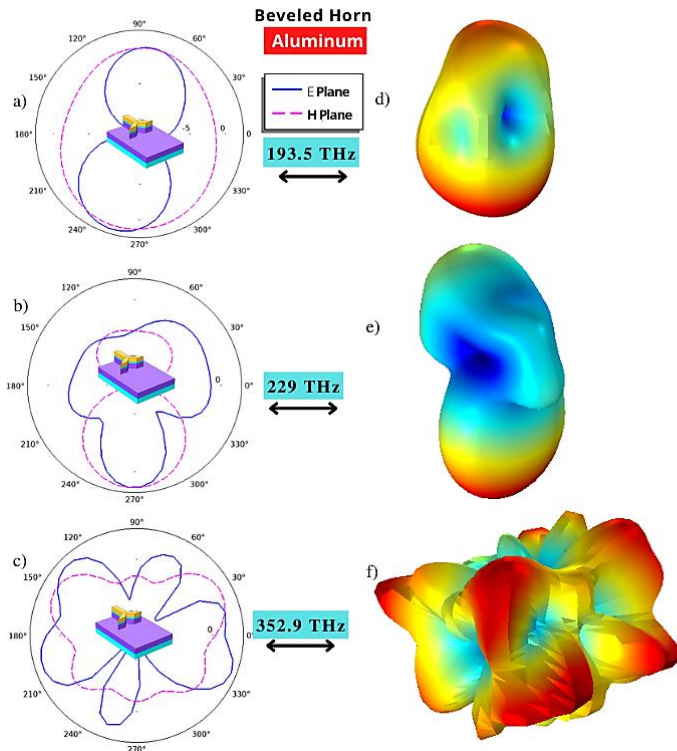


Fig. 11. Radiation diagrams of the beveled aluminum horn: in 2D (a), (b) and (c); and in 3D (d), (e) and (f).

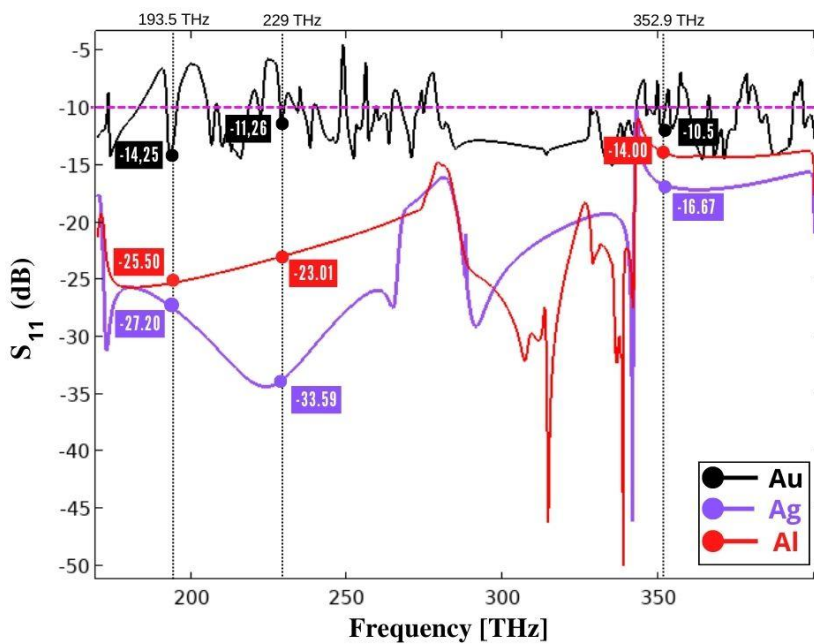


Fig. 12. Results of reflection coefficients (S_{11}) as a function of frequency for beveled horn in (Au), silver (Ag) and aluminum (Al).

Table II shows the results of the parameters: directivity, reflection coefficient and gain of the beveled horn nanoantenna.

TABLE II. RESULTS OF S_{11} , DIRECTIVITY AND GAIN OF THE BEVELED HORN

Metal	Parameters (dB)	193.5 THz	229 THz	352 THz
Au	S_{11}	-14.25	-11.26	-10.5
	Gain	2.16	7.74	4.89
Ag	S_{11}	-27.20	-33.59	-16.67
	Gain	1.90	0.74	10.34
Al	S_{11}	-25.50	-23.01	-14.00
	Gain	12.01	2.76	7.04

The results obtained in Table II are consistent with those found by the S_{11} graph and the bevel horn gain, in dB. Furthermore, there is a correspondence between the reflection coefficient result (S_{11}) shown in Fig. 12 with Table II.

Therefore, in Figs. 5, 6, 7, 9, 10 and 11, it is observed for the frequency of 352.9 THz, that the presence of side lobes in the 2D radiation diagrams caused the loss of directivity of the H-plane or chamfered sectoral horn. Furthermore, for the H plane sector horn and bevel horn, the 3D radiation diagrams at 193.5 THz and 229 THz have a well-defined central lobe. While at the frequency of 352.9 THz, the main lobe was divided regardless of the conductive material used, only with the decrease in wavelength, it appears that the nanoantennas are not directive at the frequency of 352.9 THz.

Regarding the gain, the nanoantenna with conductive silver metal showed better results than the others at the frequency of 352 THz, both for the sector horn and the bevel horn. While aluminum obtained less uniformity in the gain results in relation to the other materials when changing geometry, since the gain of the aluminum sector horn showed a decreasing behavior in the beveled nanoantenna as seen in Table II.

It is also possible to conclude that the reflection coefficient for the beveled horn was more satisfactory with the radiating element in silver and aluminum than the same in gold. Therefore, a study of other geometries is essential to verify the performance of aluminum as a conductive material.

V. CONCLUSIONS

In this paper, a plasmonic optical nanoantenna in H-plane sector horn shape is presented and fed with a hybrid plasmonic waveguide to achieve high gain with wideband operation. In addition, the variation of the conductive metal of each nanoantenna is explored to obtain savings in the material used in the construction of the antenna and to capture a satisfactory performance at the frequencies addressed. By employing the parametric study in this work, we observed the behavior of antenna geometries when changing the conductive metal into gold, silver and aluminum. The results showed that a nanoantenna made of aluminum can present satisfactory results of reflection coefficient and greater savings in manufacturing costs compared to other materials most used in the literature, but for more concrete results it is necessary to investigate new geometries to obtain the material performance in relation to gain at high frequencies. The proposed project shows the ability of a nanoantenna to

operate in a wide range of optical frequencies, as shown by the simulation results, covering all the main optical communication band bands from 150 to 400 THz and has as a future objective the construction of the nanoantenna for validation of the discussed results.

ACKNOWLEDGMENT

The authors of this work thank CNPq for the financial support and UFCG for the institutional support.

REFERENCES

- [1] J. Yan, X. Liu, C. Ma, Y. Huang, and G. Yang, "All-dielectric materials and related nanophotonic applications," *Materials Science and Engineering: R: Reports*, vol. 141, p. 100563, 2020.
- [2] N. Maccaferri, G. Barbillon, A. N. Koya, G. Lu, G. P. Acuna, and D. Garoli, "Recent advances in plasmonic nanocavities for single-molecule spectroscopy," *Nanoscale Advances*, vol. 3, no. 3, pp. 633–642, 2021.
- [3] G. Barbillon, "Latest Advances in Nanoplasmonics and Use of New Tools for Plasmonic Characterization," *Photonics*, vol. 9, no. 2, p. 112, 2022.
- [4] S.-H. Oh and H. Altug, "Performance metrics and enabling technologies for nanoplasmonic biosensors," *Nature Communications*, vol. 9, no. 1, p. 5263, 2018.
- [5] M. Dolci, J. F. Bryche, C. Leuvrey, S. Zafeiratos, S. Gree, and S. Begin-Colin, "Robust clicked assembly based on iron oxide nanoparticles for a new type of SPR biosensor," *Journal of Materials Chemistry C*, vol. 6, no. 34, pp. 9102–9110, 2018.
- [6] M. Dolci, J. Bryche, J. Moreau, C. Leuvrey, S. Begin-Colin, G. Barbillon, and B. P. Pichon, "Investigation of the structure of iron oxide nanoparticle assemblies in order to optimize the sensitivity of surface plasmon resonance-based sensors," *Applied Surface Science*, vol. 527, pp. 146773, 2020.
- [7] A. Sarychev, A. Ivanov, A. Lagarkov, and G. Barbillon, "Light Concentration by Metal-Dielectric Micro-Resonators for SERS Sensing," *Materials*, vol. 12, no. 1, p. 103, 2018.
- [8] H. Kurt, P. Pishva, Z. S. Pehlivan, E. G. Arsoy, Q. S. Mustafa, K. Bayazite, and M. Yüce, "Nanoplasmonic Biosensors: Theory, Structure, Design, and Review of Recent Applications," *Analytica Chimica Acta*, vol. 1185, p. 338842, 2021.
- [9] A. N. Masterson, B. B. Muhoberac, A. Gopinadhan, D. J. Wilde, F. T. Deiss, C. C. John, and R. Sardar, "Multiplexed and High-Throughput Label-Free Detection of RNA/Spike Protein/IgG/IgM Biomarkers of SARS-CoV-2 Infection Utilizing Nanoplasmonic Biosensors," *Analytical Chemistry*, vol. 93, no. 25, pp. 8754–8763, 2021.
- [10] H. Altug, S.-H. Oh, S. A. Maier, and J. Homola, "Advances and applications of nanophotonic biosensors," *Nature Nanotechnology*, vol. 17, no. 1, pp. 5–16, 2022.
- [11] R. Verma, R. Belgamwar, and V. Polshettiwar, "Plasmonic Photocatalysis for CO₂ Conversion to Chemicals and Fuels," *ACS Materials Letters*, vol. 3, no. 5, pp. 574–598, 2021.
- [12] S. Li, P. Miao, Y. Zhang, J. Wu, B. Zhang, Y. Du, X. Han, J. Sun, and P. Xu, "Recent Advances in Plasmonic Nanostructures for Enhanced Photocatalysis and Electrocatalysis," *Advanced Materials*, vol. 33, no. 6, p. 2000086, 2020.
- [13] V. Jain, R. K. Kashyap, and P. P. Pilla, "Plasmonic Photocatalysis: Activating Chemical Bonds through Light and Plasmon," *Advanced Optical Materials*, p. 2200463, 2022.
- [14] F. Molavi-Vardanjani, N. Hatefi-Kargan, and A. Daraei, "Performance of a Tunable Photoconductive Graphene Plasmonic Photodetector," *Zeitschrift Für Naturforschung A*, vol. 77, no. 8, pp. 813–819, 2022.
- [15] J. Zou, Y. Huang, W. Wang, C. Li, S. Wei, H. Liu, L. Luo, W. Du, K. Shen, A. Ren, and J. Wu, "Plasmonic MXene Nanoparticle-Enabled High-Performance Two-Dimensional MoS₂ Photodetectors," *ACS Applied Materials & Interfaces*, vol. 14, no. 6, pp. 8243–8250, 2022.
- [16] J. Zhang, Y. Wang, D. Li, Y. Sun, and L. Jiang, "Engineering Surface Plasmons in Metal/Nonmetal Structures for Highly Desirable Plasmonic Photodetectors," *ACS Materials Letters*, vol. 4, no. 2, pp. 343–355, 2022.
- [17] J. Chen, and G. Fengyuan, "Polarization-Switchable Plasmonic Emitters Based on Laser-Induced Bubbles," *Opto-Electronic Advances*, vol. 5, no. 8, p. 200100, 2020.
- [18] P. M. Oppeneer and V. Kapaklis, "Plasmonic lasers turn magnetic," *Nature Photonics*, vol. 16, no. 1, pp. 11–13, 2021.
- [19] N. I. Zheludev, "What diffraction limit?," *Nature Materials*, vol. 7, no. 6, pp. 420–422, 2008.
- [20] N. Li, Y. Lai, S. H. Lam, H. Bai, L. Shao, and J. Wang, "Directional Control of Light with Nanoantennas," *Advanced Optical Materials*, vol. 9, no. 1, p. 2001081, 2020.
- [21] P. Biagioni, J.-S. Huang, and B. Hecht, "Nanoantennas for visible and infrared radiation," *Reports on Progress in Physics*, vol. 75, no. 2, p. 024402, 2012.
- [22] Z.-J. Yang, R. Jiang, X. Zhuo, Y.-M. Xie, J. Wang, and H.-Q. Lin, "Dielectric nanoresonators for light manipulation," *Physics Reports*, vol. 701, pp. 1–50, 2017.
- [23] S. Lechago, C. Garcia-Meca, A. Griol, M. Kovylyna, L. Bellieres, and J. Martí, "All-Silicon On-Chip Optical Nanoantennas as Efficient Interfaces for Plasmonic Devices," *ACS Photonics*, vol. 6, no. 5, pp. 1094–1099, 2019.
- [24] D. Dregely, K. Lindfors, M. Lippitz, N. Engheta, M. Totzeck, and H. Giessen, "Imaging and steering an optical wireless nanoantenna link," *Nature Communications*, vol. 5, no. 1, 2014.
- [25] D.-I. Curiac, "Wireless Sensor Network Security Enhancement Using Directional Antennas: State of the Art and Research Challenges," *Sensors*, vol. 16, no. 4, p. 488, 2016.

- [26] T. Nagasue, T. Shinohara, S. Hasegawa, K. Imura, and K. Tawa, "Nanoantenna effect dependent on the center structure of Bull's eye-type plasmonic chip," *Optics Express*, vol. 30, no. 5, p. 7526, 2022.
- [27] M. Wersäll, R. Verre, M. Svedendahl, P. Johansson, M. Käll, and T. Shegai, "Directional Nanoplasmonic Antennas for Self-Referenced Refractometric Molecular Analysis," *The Journal of Physical Chemistry C*, vol. 118, no. 36, pp. 21075–21080, 2014.
- [28] Y. Xiong, T. Fu, D. Zhang, S. Zhang, and H. Xu, "Superradiative plasmonic nanoantenna biosensors enable sensitive immunoassay using the naked eye," *Nanoscale*, vol. 13, no. 4, pp. 2429–2435, 2021.
- [29] J. D. Ortiz, J. P. del Risco, J. D. Baena, and R. Marqués, "Extension of Babinet's principle for plasmonic metasurfaces," *Applied Physics Letters*, vol. 119, no. 16, p. 161103, 2021.
- [30] K. Delfanazari and O. L. Muskens, "Visible to Near-infrared Chip-integrated Tunable Optical Modulators Based on Niobium Plasmonic Nano-antenna and Nano-circuit Metasurface Arrays," *2022 Photonics & Electromagnetics Research Symposium (PIERS)*, 2022, pp. 924-929.
- [31] P. Spinelli, M. A. Verschuuren, and A. Polman, "Broadband omnidirectional antireflection coating based on subwavelength surface Mie resonators," *Nature Communications*, vol. 3, no. 1, p. 692, 2012.
- [32] Y. Zhang, Y. Xu, S. Chen, H. Lu, K. Chen, Y. Cao, A. E. Miroshnichenko, M. Gu, and X. Li, "Ultra-Broadband Directional Scattering by Colloidally Lithographed High-Index Mie Resonant Oligomers and Their Energy-Harvesting Applications," *ACS Applied Materials & Interfaces*, vol. 10, no. 19, pp. 16776–16782, 2018.
- [33] T. Shegai, S. Chen, V. D. Miljković, G. Zengin, P. Johansson, and M. Käll, "A bimetallic nanoantenna for directional colour routing," *Nature Communications*, vol. 2, no. 1, p. 481, 2011.
- [34] X. Zhuo, H. K. Yip, X. Cui, J. Wang, and H.-Q. Lin, "Colour routing with single silver nanorods," *Light: Science & Applications*, vol. 8, no. 1, p. 39, 2019.
- [35] M. Poblet, R. Berté, H. D. Boggiano, Y. Li, E. Cortés, G. Grinblat, S. A. Maier, and A. V. Bragas, "Acoustic Coupling between Plasmonic Nanoantennas: Detection and Directionality of Surface Acoustic Waves," *ACS Photonics*, vol. 8, no. 10, pp. 2846–2852, 2021.
- [36] P. Livreri and F. Beccaccio, "Optical Plasmonic Nanoantenna-MWCNT diode Energy Harvester for Solar Powered Wireless Sensors," *2021 IEEE Sensors*, pp. 1-4, 2021.
- [37] I. Ahmad, S. Ullah, J. Din, S. Ullah, W. Ullah, U. Habib, S. Khan, and J. Anguera, "Maple-Leaf Shaped Broadband Optical Nano-Antenna with Hybrid Plasmonic Feed for Nano-Photonic Applications," *Applied Sciences*, vol. 11, no. 19, p. 8893, 2021.
- [38] M. Khodadadi, N. Nozhat, and S. M. M. Moshiri, "Theoretical analysis of a circular hybrid plasmonic waveguide to design a hybrid plasmonic nano-antenna," *Scientific Reports*, vol. 10, no. 1, 2020.
- [39] R. Mupparapu, J. Cunha, F. Tantussi, A. Jacassi, L. Summerer, M. Patrini, A. Giugni, L. Maserati, A. Alabastri, D. Garoli, and R. P. Zaccaria, "High-Frequency Light Rectification by Nanoscale Plasmonic Conical Antenna in Point-Contact-Insulator-Metal Architecture," *Advanced Energy Materials*, vol. 12, no. 15, p. 2103785, 2022.
- [40] M. Tabatabaian, COMSOL for Engineers. Google Books, Mercury Learning and Information, 2015.
- [41] F. Duarte, J. P. N. Torres, A. Baptista, and R. A. Marques Lameirinhas, "Optical Nanoantennas for Photovoltaic Applications," *Nanomaterials*, vol. 11, no. 2, p. 422, 2021.
- [42] A. Nourmohammadi, and M. Nikoufard, "Ultra-Wideband Photonic Hybrid Plasmonic Horn Nanoantenna with SOI Configuration," *Silicon*, vol. 12, no. 1, pp. 193–198, 2019.
- [43] A. A. C. Alves, M. C. Melo, J. J. Siqueira, F. Zanella, J. R. Mejia-Salazar and C. S. Arismar, "Plasmonic Nanoantennas for 6G Intra/Inter-Chip Optical-Wireless Communications," *2020 2nd 6G Wireless Summit (6G SUMMIT)*, pp. 1-4, 2020.
- [44] L. Yousefi and A. C. Foster, "Waveguide-fed optical hybrid plasmonic patch nano-antenna," *Optics Express*, vol. 20, no. 16, p. 18326, 2012.